**Aalborg Universitet**

AALBORG UNIVERSITY
DENMARK

# A Nonlinear, Bounded and Lipchitz Continuous Distributed Active Power Sharing Control Method for Islanded AC Microgrids

Meng, Xiaoxiao; Zhou, Niancheng; Wang, Qianggang; Guerrero, Josep M.

*Published in:*
IEEE Access

*DOI (link to publication from Publisher):*
10.1109/ACCESS.2019.2900172

*Publication date:*
2019

*Document Version*
Publisher's PDF, also known as Version of record

Link to publication from Aalborg University

*Citation for published version (APA):*
Meng, X., Zhou, N., Wang, Q., & Guerrero, J. M. (2019). A Nonlinear, Bounded and Lipchitz Continuous Distributed Active Power Sharing Control Method for Islanded AC Microgrids. *IEEE Access*, *7*, 36843-36853. [8648177]. https://doi.org/10.1109/ACCESS.2019.2900172

**General rights**
Copyright and moral rights for the publications made accessible in the public portal are retained by the authors and/or other copyright owners and it is a condition of accessing publications that users recognise and abide by the legal requirements associated with these rights.

? Users may download and print one copy of any publication from the public portal for the purpose of private study or research.
? You may not further distribute the material or use it for any profit-making activity or commercial gain
? You may freely distribute the URL identifying the publication in the public portal ?

**Take down policy**
If you believe that this document breaches copyright please contact us at vbn@aub.aau.dk providing details, and we will remove access to the work immediately and investigate your claim.

IEEE Access
Multidisciplinary | Rapid Review | Open Access Journal

Received January 23, 2019, accepted February 6, 2019, date of publication February 21, 2019, date of current version April 3, 2019.

*Digital Object Identifier 10.1109/ACCESS.2019.2900172*

# A Nonlinear, Bounded and Lipchitz Continuous Distributed Active Power Sharing Control Method for Islanded AC Microgrids

**XIAOXIAO MENG[1], NIANCHENG ZHOU[1], (Member, IEEE), QIANGGANG WANG[1], (Member, IEEE), AND JOSEP M. GUERRERO[2], (Fellow, IEEE)**

[1]School of Electrical and Engineering, Chongqing University, Chongqing 400044, China
[2]Department of Energy Technology, Aalborg University, 9220 Aalborg, Denmark

Corresponding author: Qianggang Wang (qianggang1987@cqu.edu.cn)

This work was supported by the National Natural Science Foundation of China under Grant 51577018.

**ABSTRACT** In this paper, a nonlinear, bounded, distributed secondary control (DSC) method is proposed to coordinate all the distributed generators (DGs) in islanded AC microgrids (MGs). This proposed consensus-based DSC strategy can not only guarantee the restoration control of frequency and voltage but also realize an accurate active power sharing control. Through introducing a nonlinear dynamic from beta cumulative distribution function (CDF), the convergence speed of DSC is accelerated, the asymptotical convergence of DSC is ensured, and the transient overshoot of DSC is diminished compared with traditional DSC. Moreover, by ensuring the Lipchitz continuity characteristic of the control algorithm, the common chattering phenomenon in non-Lipchitz DSC scheme is eliminated. The stability and performance of the proposed DSC are also analyzed in this paper. An islanded AC microgrid test system with four inverter-based DGs is built in MATLAB/SIMULINK to further validate the effeteness of the proposed DSC strategy.

**INDEX TERMS** Nonlinear distributed secondary control, islanded microgrid, multi-agent system, Lipchitz continuity, chattering phenomenon.

## I. INTRODUCTION

Microgrid is a localized group of Distributed Generation (DG), Energy Storage System (ESS) and local loads that normally connect to and synchronous with the main grid, but also intentionally or unintentionally disconnect to islanded mode [1]. In this way, a microgrid can effectively supply emergency power, changing between islanded and connected modes. In islanded mode, the microgrid is easier to suffer from frequency and voltage deviation due to its low power capacity, weak network structure and frequent fluctuations of loads. Thus, a wide-used operation scheme called hierarchical control is implemented in islanded microgrid, and it usually has three control levels [2]–[4].

The primary control level normally adopts the $P\omega$ and $QV$ droop control strategy, or some improved forms in special application scenarios. The control effect is stabilizing voltage and frequency with some inherent deviations between reference and practical values. Then the secondary control level is implemented to compensate these deviations and further realize the active or reactive power sharing. Finally, the tertiary level can determine the optimizing and economic operation. In this paper, we mainly focus on the secondary control level.

In general, secondary control structures can be centralized [5]–[7] or distributed [8]–[17], which are two commonly utilized secondary control methods in microgrid. Comparing with the traditional centralized way, a distributed way, proposed in recent years, only requires information exchange among several neighboring local controllers, and the computation burden can be shared through all the local controllers rather than a centralized MGCC. In this way, the problems caused by single-point failure and communication congestion can be much more relieved.

Consensus-based control methods of multi-agent system (MAS) are widely used as a distributed secondary control in microgrid [10]–[17]. In [10]–[12], the traditional linear consensus feedback control scheme is used, where all the

The associate editor coordinating the review of this manuscript and approving it for publication was Xiwang Dong.



2169-3536 © 2019 IEEE. Translations and content mining are permitted for academic research only.
Personal use is also permitted, but republication/redistribution requires IEEE permission.
See http://www.ieee.org/publications_standards/publications/rights/index.html for more information.

agents reach consensus in an asymptotical convergence time. However, considering the intermittent of DGs and constantly changing of local loads, the traditional linear asymptotical convergence property may not suitable for the fast-changing operating conditions.

Base on this, some nonlinear consensus-based finite-time convergence control methods are proposed to achieve a finite settling time for the secondary control [13]–[17]. In [13] and [14], the voltage and frequency restoration control with accurate real power sharing are achieved in finite-time. In [15], a finite-time nonlinear convergence control is proposed, which considers the synchronization control for the frequency and voltage and active power sharing when microgrid having switching communication topologies. Given that there is a tradeoff between voltage regulation and reactive power sharing, a novel observer-based distributed voltage regulator involving certain reactive power sharing constraints is proposed in [16], which can realize reactive power sharing with a bounded voltage. Still a novel nonlinear consensus-based DSC method is also proposed to restore the frequency and achieve the active power sharing. Moreover, in order to accommodate the intermittent renewable generations and constantly changing load demands, a distributed, bounded and finite-time convergence secondary control is proposed in [17] by using the inverse hyperbolic tangent (tanh) nonlinear dynamic technique.

Almost all the nonlinear finite-time DSC methods proposed in the literatures above adopt some sort combining techniques of sign function, saturation function, and fractional power integrator. In most cases, these types of control algorithms are called right side non-Lipchitz functions [18]–[20]. Adopting these types of DSC methods can realize a relatively fast finite-time convergence. However, in the meantime, an inherent, non-negligible chattering phenomenon happened at steady state will be introduced in the system dynamic [21], especially in active power sharing control, which are rarely discuss in recent research papers.

The main contribution of this paper is that, we propose a nonlinear, Lipchitz-continuous, and bounded convergence secondary control method for an islanded AC microgrid to restore the frequency and voltage and meantime realize an accurate active power sharing for each DG without chattering phenomenon. Using a nonlinear dynamic inspired by the Beta CDF technique combining with the sign function and saturation function, the higher convergence speed is preserved and the transient overshot is greatly reduced comparing with the traditional DSC. Moreover, the chattering phenomenon in non-Lipchitz dynamic system is discussed, and the Lipchitz continuity is ensured to eliminate the chattering in steady state comparing with the finite time DSC in [16] and [17]. The Lyapunov function is presented to certify the Lyapunov stability of this proposed DSC method. An islanded AC microgrid test system with four inverter-based DGs in Matlab/Simulink is presented to validate the effectiveness of the proposed distributed control strategy.

The main contributions of the paper are summarized as:

1) Both output voltages and frequency of DG in the islanded microgrid are restored to their reference values while keeping active power sharing accuracy by using a nonlinear distributed control. This proposed method can greatly suppress the dynamic transient overshoot and in the meantime have a relative faster convergence speed comparing with the traditional control method.
2) Through adopting a Lipchitz continuous control scheme, the common chattering phenomena happened in the most non-Lipchitz finite-time control are totally avoided, the control accuracy is preserved.

The rest of the paper is organized as follows. Section II presents the preliminaries of graph theory and the conventional droop-based primary control scheme. Section III introduces the proposed nonlinear distributed control algorithm for frequency restoration and active power sharing control. Section IV provides the Lyapunov stability proof and discusses the chattering phenomenon in non-Lipchitz dynamic system and its elimination method to improve the dynamic performance. Section V discusses the simulation results, and Section VI provides the conclusion.

## II. PROBLEM FORMATION AND PRELIMINARIES

### A. PRABLEM FORMATION

In this paper, we mainly focus on an islanded AC microgrid with $N$ inverter-based DGs. Each DG consists of an ideal DC source, a DC/AC inverter, and an Inductance-Capacitance-Inductance (LCL) filter. Its basic control diagram includes inner voltage and current control loops as well as the primary and proposed secondary control scheme, which can be presented in Fig. 1.

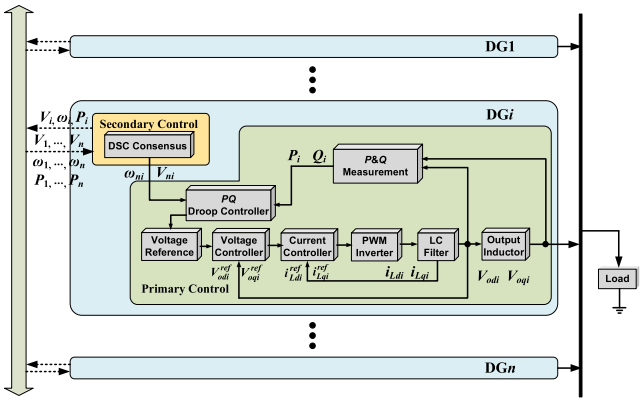


**FIGURE 1.** The control loops for a multi inverter-based DG microgrid.

As seen in Fig. 1, the current, voltage, and power control loops are employed in each DG. The primary control procedure is implemented during the power control loop with the nominal set points $V_{ni}$ and $\omega_{ni}$ generated by the secondary control procedure. Then, with the reference values, $V_{odi}^{ref}$ and $V_{oqi}^{ref}$, provided by the power loop, the outer voltage loop generates the current reference, $i_{Ldi}^{ref}$ and $i_{Lqi}^{ref}$, for the

inner current loop. Finally, the current error is calculated and further used to regulate the output of the inverter by the sinusoidal pulse width modulation (SPWM) mode [1].

In this paper, we propose a nonlinear consensus-based DSC method through the information exchanges among the several neighboring DGs in a sparse communication network to update $V_{ni}$ and $\omega_{ni}$ in each primary control process, and further restore the output voltage $V_i$ and frequency $\omega_i$, to their reference values. The reference values, $V_{ref}$ and $\omega_{ref}$, are provided by a so-called virtual leader DG, which can be offered by the main grid in grid-connected mode or obtained by a specific command DG in islanded mode.

The output impedance characteristic of each DG is highly inductive due to the *LCL* filter circuit, so that the following conventional $P\omega$ and $Q$-$V$ droop-based primary control strategy can be used in the power control loop [1], [3]:

$$\begin{cases} \omega_i = \omega_{ni} - K_{Pi}P_i \\ \begin{cases} V_i = V_{ni} - K_{Qi}Q_i \\ V_{odi} = V_i \end{cases} \end{cases} \tag{1}$$

where $V_{odi}$ and $\omega_i$ are the output voltage magnitude and frequency respectively, here we choose the d-axis output voltage orientation principle. $P_i$ and $Q_i$ are the average active and reactive powers after low-pass filters, $K_{Pi}$ and $K_{Qi}$ are the corresponded droop coefficients, and their magnitudes are commonly designed according to their rating power $P_{i,\max}$ and $Q_{i,\max}$

### B. PRELIMINARIES OF COMMUNICATION NETWORK

The communication structure of an microgrid with multi DGs is a typical multi-agent system, where each DG follows the consensus-based convergence rule. Here the algebraic digraph theory is introduced in [22], and the communication network can be modeled as a directed graph $\boldsymbol{G}(\boldsymbol{v}, \boldsymbol{\varepsilon}, \boldsymbol{A})$, where $\boldsymbol{v} = \{v_1, v_2, \ldots, v_N\}$ denotes the node set of DG, $\varepsilon \subseteq \boldsymbol{v} \times \boldsymbol{v}$ denotes the communication link, and $\boldsymbol{A} = (a_{ij})N \times N$ denotes the weighted adjacency matrix. What's more, the adjacent weight $a_{ii} = 0$, $a_{ij} \geq 0$, and $a_{ij} > 0$ if and only if the link $(v_i, v_j) \in \boldsymbol{\varepsilon}$

The set of DG$_i$'s neighbors is given by $N_i = \{v_j \in \boldsymbol{v}: (v_i, v_j) \in \boldsymbol{\varepsilon}\}$. The Laplacian matrix of $\boldsymbol{A}$ is defined as $\boldsymbol{L}(\boldsymbol{A}) = (l_{ij})N \times N$, $l_{ij} = -a_{ij}$, $i \neq j$, and $l_{ij} = \sum_{k=1}^{N} a_{ik}$ for all $i$, which satisfies $\boldsymbol{L}(A)\boldsymbol{1}_N = 0$ with $\boldsymbol{1}_N = (1, \ldots, 1)^T \in \boldsymbol{R}^N$

Diagonal matrix $\boldsymbol{D} = \text{diag}\{a_{10}, \ldots, a_N\}$ is called the virtual leader adjacency matrix, where $a_i > 0$ if follower DG$i$ is connected to the leader DG0 through the link $(v, v_i)$, otherwise $a_i = 0$.

## III. PROPOSED DISTRIBUTED SECONDARY CONTROL

Much researches have concluded that the dynamics of the voltage and current control loops are much faster than the dynamics of the power control loop if the whole control parameters are well set [23]. In other words, a typical AC microgrid with multi inverter-based DGs is a multi-time scale system and processes a high time-separating dynamics. Thus, in this paper, we mainly focus on the stability and dynamic performance issue of the power control loop, and simply implement the traditional PI controllers for the voltage and current inner control loops.

Differentiating the equations in (1) yields

$$\begin{cases} \dot{\omega}_{ni} = \dot{\omega}_i + K_{Pi}\dot{P}_i = u_{\omega i} + u_{Pi} \\ \dot{V}_{ni} = \dot{V}_i + K_{Qi}\dot{Q}_i = u_{Vi} + u_{Qi} \end{cases} \tag{2}$$

where $u_{\omega i} = \dot{\omega}_i$, $u_{Vi} = \dot{V}_i$, $u_{Pi} = K_{Pi}\dot{P}_i$, and $u_{Qi} = K_{Qi}\dot{Q}_i$ are the DSC controllers outputs for the frequency, voltage, active power and reactive power, respectively.

Now that the nominal set points for the primary power controller can be designed as,

$$\begin{cases} \omega_{ni} = \int (u_{\omega i} + u_{Pi})dt \\ V_{ni} = \int (u_{Vi} + u_{Qi})dt \end{cases} \tag{3}$$

Noticing that in an islanded AC microgrid, the frequency is a global variable, but the output voltages of DGs are local variables and may be somehow different. Therefore, there is always an inherent contradiction existing between the precise voltage regulation and reactive power sharing especially in low-voltage MGs [1], [12]. In this paper, we mainly focus on the precise voltage regulation.

Thus, we use a traditional DSC controller to restore the output voltages of all DGs, and meanwhile design a proposed nonlinear DSC method to faster restore the frequency and realize an accurate active power sharing. The control objectives can be expressed as follows.

1) All DGs' frequency and voltage regulation can be achieved asymptotically, i.e,

$$\lim_{t\to\infty} |\omega_i(t) - \omega_{ref}| = 0, \quad \lim_{t\to\infty} |V_i(t) - V_{ref}| = 0, \forall i. \tag{4}$$

2) The accurate active power sharing can also be achieved as below,

$$\lim_{t\to\infty} |K_{Pi}P_i - K_{Pj}P_j| = 0, \quad \forall i \neq j \tag{5}$$

3) The reactive power control inputs, $u_{Qi}$, can be adopted from [12], as $u_{Qi} = -K_{Qi}(\omega_c Q_i + \omega_c q_i)$, where $\omega_c$ is the cutoff frequency of the low-pass filters, $K_{Qi}$ is the reactive droop coefficient and $q_i$ is the instantaneous reactive power component.

### A. PROPOSED NONLINEAR DSC METHOD FOR FREQUENCY RESTORATION AND ACCURATE ACTIVE POWER SHARING

In a traditional droop-based AC microgrid, the primary control can automatically achieve the active power sharing but having the inherent frequency deviation. However, simply implementing the secondary frequency control without adding the auxiliary active power control may lead to inaccurate active power sharing. The restoration control of frequency and active power sharing control should be considered thoroughly as an integral.

In order to faster restore the system's frequency and realize an accurate active power sharing, a nonlinear consensus-based DSC method is designed as follow.

We first calculate the global errors of frequency and active power for DG$i$ through the communication networks, $\boldsymbol{G}(\boldsymbol{A}^{\omega})$ and $\boldsymbol{G}(\boldsymbol{A}^{P})$

$$\begin{cases} e_{\omega i} = \sum_{j\in N_i^{\omega}} a_{ij}^{\omega}(\omega_i - \omega_j) + a_{i0}^{\omega}(\omega_i - \omega_{ref}) \\ e_{Pi} = \sum_{j\in N_i^{P}} a_{ij}^{P}(K_{Pi}P_i - K_{Pj}P_j) \end{cases} \tag{6}$$

where the adjacent weights of communication network for frequency $\boldsymbol{G}(\boldsymbol{A}^{\omega})$ and active power $\boldsymbol{G}(\boldsymbol{A}^{P})$ are $a_{ij}^{\omega} \in R^{N\times N}$ and $a_{ij}^{P} \in R^{N\times N}$ respectively. The corresponding adjacent weights of leaders for frequency is $a_{i0}^{\omega}$ where $a_{i0}^{\omega} > 0$ if and only if DG$i$ can access to the reference values $\omega_{ref}$, otherwise they equal to zero. Here we assume only one DG can be connected to the virtual leader $\mathrm{DG}_0$.

To achieve a fast convergence speed frequency regulation and accurate active power sharing, as well further avoid the transient overshoot and chattering phenomenon, a nonlinear and right-side Lipchitz continuity dynamic function is adopted to construct controllers, where the idea is inspired by the Beta Cumulative Distribution Function (CDF). Thus, the DSC outputs $u_{\omega i}$ and $u_{Pi}$ can be designed as,

$$\begin{cases} u_{\omega i} = -C_{\omega}F_B(e_{\omega i}, \beta_{\omega}, r_{\omega}) \\ u_{Pi} = -C_P F_B(e_{Pi}, \beta_P, r_P) \end{cases} \tag{7}$$

where $F_B(\cdot)$ is self-defined function which can be viewed as a special case of an Beta PDF function (case: assuming shape parameters $\alpha = 1$ and $\beta \geq 1$), $C_{\omega}$, $C_P > 0$ are the proportion gains, $r_{\omega}$, $r_P > 0$ are the scaling parameters, and $\beta_{\omega}$, $\beta_P \geq 1$ are the shape parameters. The detail expression of $F_B(\cdot)$ can be further shown as (8) and (9),

$$F_B(x, \beta, r) = sign(x)\cdot(1 - (1 - r\,\mathrm{sat}_{1/r}(|x|))^{\beta}) \tag{8}$$

where sign $(\cdot)$ is the sign function, and sat $(\cdot)$ is the saturation function defined as,

$$\mathrm{sat}_{1/r}(u) = \begin{cases} u|u| \leq \dfrac{1}{r} \\ \mathrm{sign}(u)\dfrac{1}{r}|u| > \dfrac{1}{r} \end{cases} \tag{9}$$

Note that the dynamic system in (8) become the traditional linear DSC system with saturation constant $1/r$ when $\beta = 1$. The further detailed certification process for the asymptotical stability is given in Section IV, here we obtain the following conclusion.

*Theorem 1:* If diagraph $\boldsymbol{G}(\boldsymbol{A}^{P})$ and $\boldsymbol{G}(\boldsymbol{A}^{\omega})$ are strongly connected, and there is at least one DG can access to the virtual leader reference $\omega_{ref}$, then the droop control law (1) combining with the proposed DSC method, (7) and (8), can guide all DGs' frequencies to their reference values asymptotically while maintaining the active power sharing accuracy.

### B. DISTRIBUTED SECONDARY CONTROL FOR VOLTAGE RESTORATION

As for the voltage restoration control, what we concern in this paper is that we realize the voltage restoration in a relative slow time scale. Since we have already regulated all DGs' frequency with a faster convergence speed while maintaining the active power sharing [16], [17]. If we can design the frequency and voltage controllers separately at different convergence pace, the inherent coupling between voltage and frequency can be reduced to some extent especially when the line impedance are not so matched.

Therefore, we simply use the traditional linear DSC asymptotic convergence to solve the leader-followers' consensus for voltage [11], so the continuous-time distributed controllers can be constructed as

$$u_{Vi} = -C_V e_{Vi} \tag{10}$$

where $C_V > 0$, and $e_{Vi}$ can be derived as,

$$e_{Vi} = \sum_{j\in N_i^{V}} a_{ij}^{V}(V_i - V_j) + a_{i0}^{V}(V_i - V_{ref}) \tag{11}$$

here the adjacent weights of communication network for voltage $G(A^{V})$ is $a_{ij}^{V} \in R^{N\times N}$. The corresponding adjacent weights for voltage leader is $a_{i0}^{V}$ and we also assume only one DG can access to the voltage reference $V_{ref}$

## IV. STABILITY AND PERFORMANCE ANALYSIS

In this section, the Lyapunov method is used at first to illustrate the stability issue of ***Theorem* 1** for frequency and active power. Then, we further discuss a common problem happened in non-Lipchitz dynamic control algorithm called chattering phenomenon and analyze its negative effects to the system performance.

### A. PROOF OF THEOREM 1

In order to better derive the stability of (7), first let $\bar{\omega} = [\bar{\omega}_1, \bar{\omega}_2, \ldots, \bar{\omega}_n]^T$, with $\bar{\omega}_i = \omega_i - \omega_{ref}$, $x = [x_1, x_2, \ldots, x_n]^T$, with $x_i = K_{Pi}\cdot P_i$, and $y = [y_1, y_2, \ldots, y_n]^T$, with $y_i = e_{\omega i}$, $z = [z_1, z_2, \ldots, z_n]^T$, with $z_i = e_{Pi}$

So here we can get $y_i = \sum_{j\in N_i^{P}} a_{ij}^{\omega}(\bar{\omega}_i - \bar{\omega}_j) + a_{i0}^{\omega}\bar{\omega}_i$, and $z_i = \sum_{j\in N_i^{P}} a_{ij}^{P}(x_i - x_j)$, further presented in matrix form as $y=(\boldsymbol{L}^{\omega} + \boldsymbol{D}^{\omega})\bar{\omega}$, $z = \boldsymbol{L}^{P}x$

We differential the two side of the expressions above as,

$$\begin{cases} \dot{y} = -sign(y)C_{\omega}(\boldsymbol{L}^{\omega}+\boldsymbol{D}^{\omega})(1-(1 - r_{\omega}\mathrm{sat}_{1/r_{\omega}}(|y|))^{\beta_{\omega}}) \\ \dot{z} = -sign(z)C_P\boldsymbol{L}^{P}(1 - (1 - r_P\mathrm{sat}_{1/r_P}(|z|))^{\beta_P}) \end{cases} \tag{12}$$

Choosing the Lyapunov candidates $V = V(t, y) + V(t, z)$ where $V(t, y)$ and $V(t, z)$ can be chosen respectively as

$$\begin{cases} V(y,t) = \sum_{i=1}^{n}[r_\omega|y_i| - \frac{1}{\beta_\omega+1} \\ \qquad \times (1-(1-r_\omega \mathrm{sat}_{1/r_\omega}|y_i|)^{\beta_\omega+1})] \\ V(z,t) = \sum_{i=1}^{n} w_i[r_P|z_i| - \frac{1}{\beta_P+1} \\ \qquad \times (1-(1-r_P \mathrm{sat}_{1/r_P}|z_i|)^{\beta_P+1})] \end{cases} \tag{13}$$

where $w_i \in \boldsymbol{w}$ is a positive column vector element meeting the requirement as $\boldsymbol{w}^T \boldsymbol{L}(\boldsymbol{A}) = 0$.

The time derivative function of Lyapunov function $V(y, t)$ can be denoted as

$$\begin{aligned} \dot{V}(t,y) = &-C_\omega r_\omega [1-(1-r_\omega \mathrm{sat}_{1/r_\omega}|y|)^{\beta_\omega}]^T \\ &\times (L^\omega + D^\omega)[1-(1-r_\omega \mathrm{sat}_{1/r_\omega}|y|)^{\beta_\omega}] \end{aligned} \tag{14}$$

where $V(t, y) \geq 0$ and is globally positive defined giving that $\partial V(t, y)/\partial y \geq 0$ and $V(t, 0) = 0$. The detail theoretical analysis of (14) is given in ***Lemma* 1**. According to the definition of strongly connected graph in ***Lemma* 2**, $\boldsymbol{L}^\omega + \boldsymbol{D}^\omega$ is a positive defined matrix, so we simply get $\dot{V}(t, y) \leq 0$

Similarly, we obtain $V(t, z) \geq 0$ and is globally positive defined Its time derivative function can be further written as

$$\begin{aligned} \dot{V}(t,z) = &-C_P r_P (1-(1-r_P \mathrm{sat}_{1/r_P}|z|)^{\beta_\omega})^T \\ &\cdot dig(w) L^P (1-(1-r_P \mathrm{sat}_{1/r_P}|z|)^{\beta_\omega}) \\ \leq &-C_P r_P \lambda_2(M) \sum_{i=1}^{n} (1-r_P \mathrm{sat}_{1/r_P}|z_i|)^{\beta_\omega})^2 \leq 0 \end{aligned} \tag{15}$$

where $M$ is called mirror matrix of dig($\boldsymbol{w}$) $L^P$, which can be denoted as 1/2(dig($\boldsymbol{w}$)$\boldsymbol{L}^P$+ $(\boldsymbol{L}^P)^T$ dig($\boldsymbol{w}$)), $\lambda_2$ is the second smallest positive eigenvalue of $M$ [24].

Thus combining (14) and (15), we yield,

$$\dot{V} = \dot{V}(t, y) + \dot{V}(t, z) \leq 0 \tag{16}$$

For the case of $\dot{V} = 0$, we yield $(y^T, z^T)^T = (0, 0)^T$. Since $y = (\boldsymbol{L}^\omega + \boldsymbol{D}^\omega)\bar{\omega}$ with the positive definite matrix $\boldsymbol{L}^\omega + \boldsymbol{D}^\omega$, then $\bar{\omega}_i = 0$ and thus $\omega_1 = \omega_2 = \ldots = \omega_N = \omega_{ref}$. Moreover, since $z = -\boldsymbol{L}^P P$ with rank($\boldsymbol{L}^P$) $= N - 1$ due to the strongly connection of $\boldsymbol{G}(\boldsymbol{A}^P)$, $z =$ implies that $K_{P1}P_1 = K_{P2}P_2 = \ldots = K_{PN}P_N$. Therefore, the frequency and active power control problem can be solved within a finite time.

### B. CHATTERING PHENOMENON ANALYSIS

The traditional linear DSC (TDSC) algorithm, the finite time DSC (FDSC) algorithms in [16] and [17], and the proposed nonlinear DSC (PDSC) algorithm in this paper are chosen as objects, to further compare their dynamics.

The general form of traditional DSC consensus method with saturation function can be shown as,

$$\begin{cases} u_1(P_i) = -k_1 \mathrm{sat}_{\delta_1}(e(P_i)) \\ e(P_i) = \sum_{j \in N_i^P} a_{ij}^P (K_{Pi}P_i - K_{Pj}P_j) \end{cases} \tag{17}$$

where $k_1 > 0$ and $e(P_i)$ represents global error of DG$i$ active power

In order to realize a finite time frequency control and accurate active power sharing with a relative fast convergence speed, in the meantime suppress the transient overshoot, some sort combination technique of sign function, bounded control (saturation function or tanh function) and fractional power integrator are proposed in [16] and [17].

The general dynamic control scheme for active power sharing [16] can be simply presented as,

$$\begin{cases} u_2(P_i) = -\mathrm{sat}_{\delta_2}(k_2 e(P_i) - k_3 \mathrm{sign}(e(P_i))^{\alpha_1}) \\ e(P_i) = \sum_{j \in N_i^P} a_{ij}^P (K_{Pi}P_i - K_{Pj}P_j) \end{cases} \tag{18}$$

where $k_2 > 0$, $k_3 > 0$, $0 \leq \alpha_1 \leq 1$, $\mathrm{sign}(\cdot)^\alpha = \mathrm{sign}(\cdot)|\cdot|^\alpha$, and $\mathrm{sat}_\delta(\cdot) = \delta \mathrm{sign}(\cdot)$ with Saturation constant $\delta$.

In [17], however, the tanh function combined with fractional power integrator technique is proposed in control scheme, which can be simply shown as,

$$\begin{cases} u_3(P_i) = -k_4 f_e(P_i) \\ f_e(P_i) = \sum_{j \in N_i^P} a_{ij} \mathrm{sign}(\tanh(k_5(K_{Pi}P_i - K_{Pj}P_j)))^{\alpha_2} \end{cases} \tag{19}$$

where $k_4 > 0$, $k_5 > 0$, $0 \leq \alpha_2 \leq 1$.

However, it is known that there is an undesirable oscillation around the equilibrium, called *chattering phenomenon*, usually occur in the finite-time convergence. Because of their right-side non-Lipschitz dynamics, the uniqueness of solutions for such systems is thus not guaranteed even in forward time [25], [26]. The further explanation of Lipchitz continuity characteristic can be seen in ***Lemma* 3**. In this paper, we propose a bounded Lipschitz dynamic DSC, which can at best emulate the finite-time consensus but also avoiding chattering phenomenon. In this section, we rewrite the active power sharing control method of 12 as follow.

$$\begin{cases} u_4(P_i) = -C_P sign(e(P_i)) \\ \qquad \cdot (1-(1-r_P \mathrm{sat}_{1/r_P}(|e(P_i)|))^{\beta_P}) \\ e(P_i) = \sum_{j \in N_i^P} a_{ij}^P (K_{Pi}P_i - K_{Pj}P_j) \end{cases} \tag{20}$$

where $C_P > 0$, $r_P > 0$, $\beta_P \geq 1$.

In order for easier comparison and explanation, here we only investigate a basic analysis scenario with 2 DGs and 0-1 adjacent weight; the analysis result can be easily extended to the multi-DGs scenario. The differential equations of (17)-(20) can be simply obtained and further represented as (21),

$$\begin{cases} \partial u_1(P_i)/\partial e(P_i) = \begin{cases} -k_1 & |e(P_i)| \leq \delta_1 \\ 0 & |e(P_i)| > \delta_1 \end{cases} \\ \partial u_2(P_i)/\partial e(P_i) = \begin{cases} -k_2 - k_3\alpha_1 |e(P_i)|^{\alpha_1 - 1} \\ \qquad |e(P_i)| \leq M(\delta_2) \\ 0 \quad |e(P_i)| > M(\delta_2) \end{cases} \\ \partial u_3(P_i)/\partial e(P_i) = -\alpha_2 k_4 k_5 |\tanh(e(P_i))|^{\alpha_2 - 1} \\ \qquad \times \left(1 - \tanh^2(e(P_i))\right) \\ \partial u_4(P_i)/\partial e(P_i) = -C_P \beta_P r_P (1 - r_P |e(P_i)|)^{\beta_P - 1} \end{cases} \tag{21}$$

where $M(\delta_2)$ is the saturation constant corresponding to $\delta_2$

The control algorithm for active power sharing control of $u_4(P_i)$ in this paper has different dynamics with different shape parameters $\beta_P$ according to (20), the result can be presented in Fig. 2(a), here we set scaling parameter $r_P = 1$. The corresponding derivative functions of (20) and its dynamic performance can be depicted in Fig. 2(b).

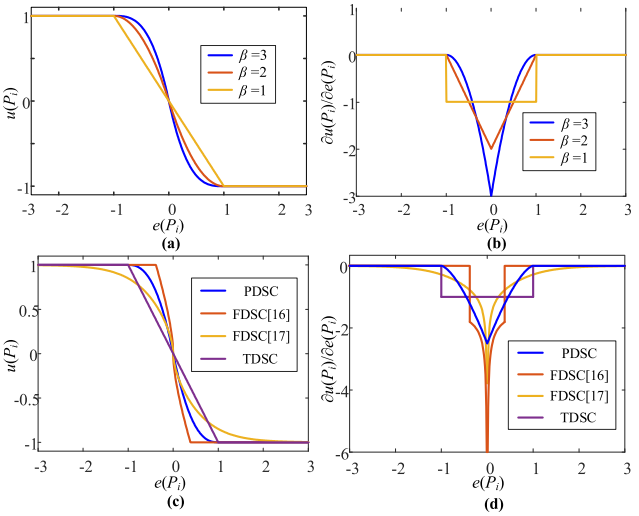


**FIGURE 2.** Dynamic behaviors of different DSC scheme algorithms. (a) PDSC dynamic function. (b) PDSC differential function. (c) Dynamic functions comparison. (d) Differential functions comparison.

In Fig. 2(c), we compare the dynamics of the TDSC method with saturation function ($k_1 = 1, \delta_1 = 1$), the FDSC method in [16] and [17] ($k_2 = k_3 = k_4 = k_5 = 1, \alpha_1 = \alpha_2 = 0.5, \delta_2 = 1$), and the PDSC method in this paper ($r_P = 1, \beta_P = 2.5$). Fig. 2(d) further depicts their differential functions.

As seen in Fig. 2(a) and 2(b), adopting proposed DSC method for active power control in this paper, the active power controller may have relative higher convergence speed and acceleration with higher shape parameter $\beta_P$, especially when $e(P_i) \to 0$.

In Fig. 2(c), the result shows that FDSC in [16] and [17] and PDSC in this paper have relatively similar dynamic due to their nonlinear characteristics comparing with the TDSC. However, in Fig. 2(d), the results clearly shows that, the FDSC method in [16] and [17] may have infinity convergence acceleration ($\partial u_2(P_i)/\partial e(P_i) \to \infty$ and $\partial u_3(P_i)/\partial e(P_i) \to \infty$) when $e(P_i) \to 0$. But the convergence acceleration of PDSC in this paper is bounded with $e(P_i) \to 0$ at this case ($|\partial u_4(P_i)/\partial e(P_i)| < M$ with $M = C_P r_P \beta_P$). In other words, according to the ***Lemma* 3** and ***Lemma* 4** in Appendix, the active power controller of FDSC in [16] and [17] satisfy the non-Lipchitz condition since $\partial u_4(P_i)/\partial e(P_i) \to \infty$ at $e(P_i) \to 0$, and PDSC in this paper is a Lipchitz continuous control method. This means that the FDSC scheme in [16] and [17] cannot thoroughly eliminate the chattering phenomena of active power sharing control dynamics. The detail validation can be seen in Section V.

### C. TRADEOFF BETWEEN TIME-DELAY AND PERFORMANCE

The time-delay effects are not theoretical analyzed in this paper due to the high nonlinear characteristic of PDSC. However, according to the research of [22], the general conclusion of time-delay effects can be provided. That is the maximum tolerant communication time-delay $\tau$ is inversely proportional to the maximum eigenvalue of Laplace matrix $\lambda_{max}$. Which can be simply presented as follow.

$$\tau \leq \frac{k}{\lambda_{max}} \tag{22}$$

Furthermore, the maximum eigenvalue $\lambda_{max} \leq 2d_{max}(G)$ according to the Gersgorin theorem, where $d_{max}(G)$ is the maximum note's out-degree of graph $G$. This means that the networks with nodes that have relatively high out-degrees cannot tolerate relatively high communication time-delays. As a result, we can simply scale down the weights of a digraph so that an arbitrary large time-delay $\tau > 0$ can be tolerated. The problem is that the convergence speed can be greatly reduced if we scale down the weights. In other words, there is always a *tradeoff* between robustness of a protocol to time-delays and its convergence speed.

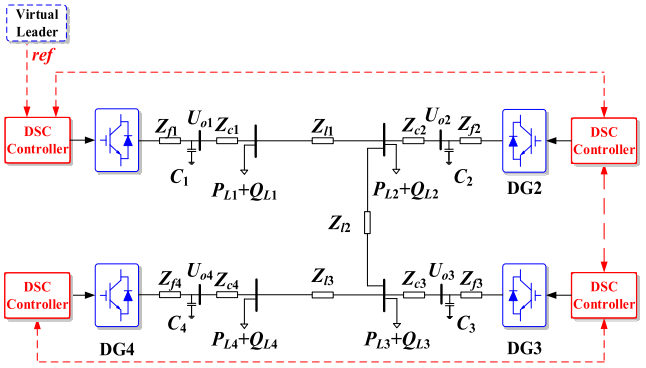


**FIGURE 3.** Islanded microgrid test system.

## V. SIMULATION VALIDATION

In order to verify the effectiveness of the proposed DSC strategy, a 380V/50Hz islanded microgrid test system including four inverted-based DGs and four local loads, is built in Matlab/SimPowerSystems, which can be shown in Fig. 3. The specifications of the DGs, lines, and loads are summarized in Table 1.

We choose the communication network with 0-1 weight as the unified digraph shown in Fig. 4. Then the associated adjacency matrices for frequency, voltage and active power are $\boldsymbol{A}^{\omega} = \boldsymbol{A}^{V} = \boldsymbol{A}^{P} = [0, 1, 0, 0; 1, 0, 1, 0; 0, 1, 0, 1; 0, 0, 1, 0]$. Here we assume only DG1 can access to the reference values of frequency and voltage, then the leader adjacency matrixes for frequency and voltage are $\boldsymbol{D}^{\omega} = \boldsymbol{D}^{V} = \text{diag}[1, 0, 0, 0]$. The proportion constants, $C_{\omega}$, $C_V$ and $C_P$, can be

**TABLE 1. Parameter values for the test system.**

| DG1 | | DG2 | | DG3 | | DG4 | |
|---|---|---|---|---|---|---|---|
| $R_{C1}$ | 0.03Ω | $R_{C2}$ | 0.03Ω | $R_{C3}$ | 0.03Ω | $R_{C4}$ | 0.03Ω |
| $L_{C1}$ | 2mH | $L_{C2}$ | 2mH | $L_{C3}$ | 2mH | $L_{C4}$ | 2mH |
| $K_{P1}$ | 13e-5 | $K_{P2}$ | 9.4e-5 | $K_{P3}$ | 13e-5 | $K_{P4}$ | 9.4e-5 |
| $K_{Q1}$ | 1e-3 | $K_{Q2}$ | 0.8e-3 | $K_{Q3}$ | 1e-3 | $K_{Q4}$ | 0.8e-3 |
| **LINE1** | | LINE2 | | | LINE3 | | |
| $R_{L1}$ | 0.64Ω | $R_{l2}$ | 0.51Ω | | $R_{l3}$ | 0.58Ω | |
| $L_{L1}$ | 1.32mH | $L_{l2}$ | 1.05mH | | $L_{l3}$ | 1.21mH | |
| **LOAD1** | | LOAD2 | | LOAD3 | | LOAD4 | |
| $P_{L1}$ | 19kW | $P_{L2}$ | 18kW | $P_{L3}$ | 22kW | $P_{L4}$ | 17kW |
| $Q_{L1}$ | 19kVar | $Q_{L2}$ | 18kVar | $Q_{L3}$ | 22kVar | $Q_{L4}$ | 17kVar |

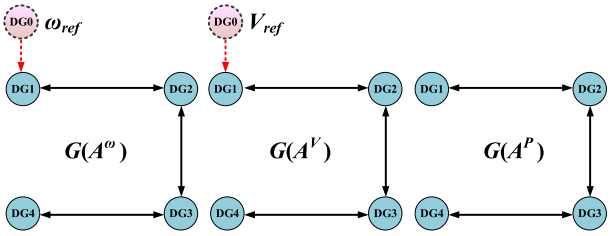


**FIGURE 4. Communication digraphs for $G(A^{\omega})$, $G(A^{V})$ and $G(A^{P})$ with fixed topology.**

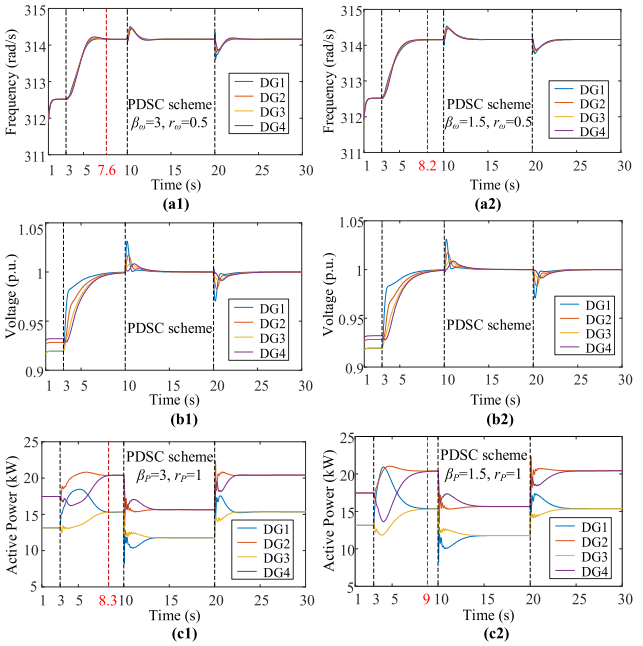


**FIGURE 5. State outputs under the PDSC scheme in case of load variation (the-red dashed lines show the convergence time of frequency and active power). (a1) and (a2) frequency response. (b1) and (b2) voltage response. (c1) and (c2) active power response.**

selected accordingly. Usually, small constant values may lead to slow convergence speed but have relative good transient response, thus we need to make a tradeoff between these two performance indexes. Here we simply choose $C_{\omega} = 4$, $C_V = 6$, and $C_P = 2$.

The simulation results will be performed in three scenarios: 1) load variation, 2) plug and play, 3) performance with communication time delays Some comparisons among the proposed distributed secondary control (PDSC) scheme, the proposed finite time distributed secondary control (FDSC) scheme in [16] and [17], and the traditional asymptotic distributed secondary control (TDSC) scheme will be given under the same scenario.

### *A. LOAD VARIATION*

The effectiveness of the proposed PDSC scheme, especially for the fast convergence speed, the bounded inputs, and the good performance to the chattering phenomenon are verified in case of load variation.

#### 1) GENERAL PERFORMANCE

At first, only the primary control is implemented. Then the PDSC are activated at $t = 3$s. The results are shown in Fig. 5. Here we set $r_{\omega} = 0.5$, $r_P = 1$, and $\beta_{\omega} = 3$, $\beta_P = 3$ for Fig. 5(a1)-(c1), $\beta_{\omega} = 1.5$, $\beta_P = 3$ for Fig. 5(a2)-(c2) respectively. As seen, the primary control could guarantee accurate active power sharing according to their droop coefficients, at meantime, keep all the frequencies convergence to a same value 312.5rad/s. However, the voltages are distributed between 0.9 to 0.95 p.u. This is because the frequency is a global value but voltage is a local value.

Moreover, all the output voltages and frequencies are less than the nominal values due to the inherent droop characteristics. After $t = 3$s, the frequency and voltage of all DGs can be gradually restored to their nominal values (i.e., $V_{ref} = 1$p.u. and $\omega_{ref} = 314.15$rad/s) as well the accurate active power sharing can be maintained in steady state according to the PDSC control strategy. Since the Load 1 is disconnected from the system at t = 10s, and reconnected to the system at 20s, Fig. 5 also shows that the PDSC scheme can keep the voltage and frequency of DGs at the nominal values while keeping accurate active power sharing response to both load connection and disconnection.

We further investigate the system dynamic under different shape parameter $\beta$ by comparing the Fig. 5(a1)-(c1) with Fig. 5(a2)-(c2). It is obvious that adopting higher $\beta$ value can have a little fast convergence speed and lower transient overshoot. However, as stated in section IV, Higher $\beta$ means higher convergence acceleration, which will in turn, makes the system more vulnerable to the oscillation in the steady state.

#### 2) TDSC SCHEME WITH OR WITHOUT SATURATION FUNCTION

By setting $\beta_{\omega} = 1$, $\beta_P = 1$, we obtain the general TDSC scheme with saturation constant $1/r_{\omega}$ and $1/r_P$, and if we further set $r_{\omega}, r_P \to 0$, the PDSC scheme becomes the TDSC without saturation function.

As seen in Fig. 6(a1) and (c1), the convergence time of $\omega$ and $P$ with saturation function are, respectively, 9.1s and 9.5s, while those in Fig. 6(a2) and (c2) are obviously no smaller

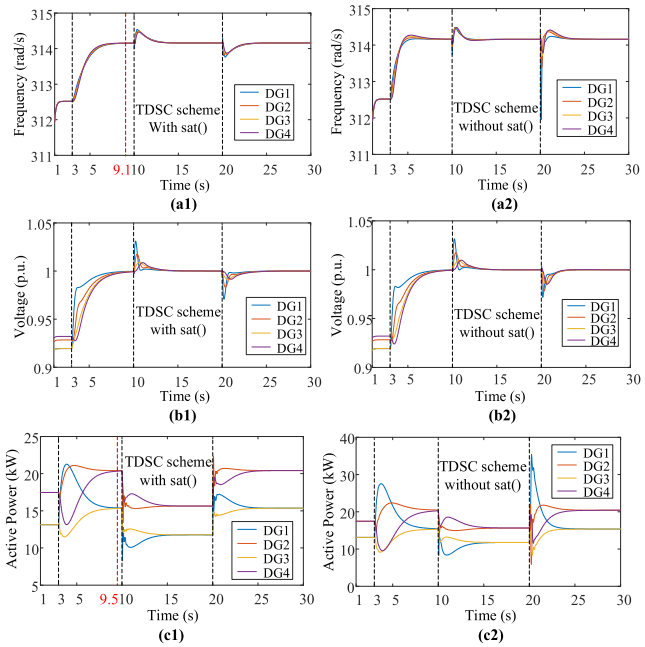


**FIGURE 6.** State outputs under the TDSC scheme with and without saturation function in case of load variation (the-red dashed lines show the convergence time of frequency and active power). (a1) and (a2) frequency response. (b1) and (b2) voltage response. (c1) and (c2) active power response.

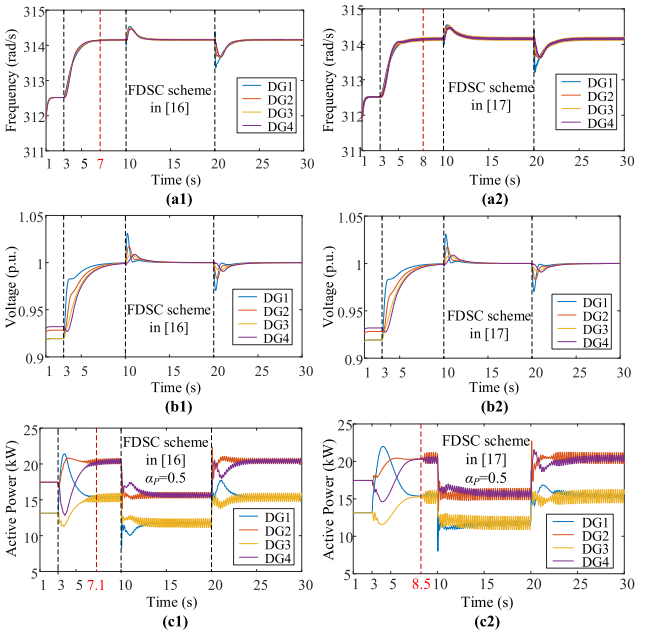


**FIGURE 7.** State outputs under the FDSC scheme in case of load variation (the-red dashed lines show the convergence time). (a1) and (a2) frequency response. (b1) and (b2) voltage response. (c1) and (c2) active power response.

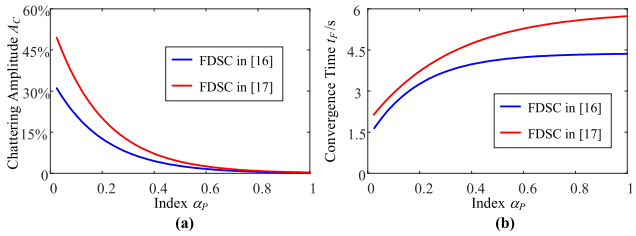


**FIGURE 8.** Chattering amplitude $A_C$ and finite convergence time $tF$ versus fractional index $\alpha_P$ curves under the FDSC schemes in [16] and [17]. (a) $A_C$ $\alpha_P$ curve. (b) $t_F$ $\alpha_P$ curve.

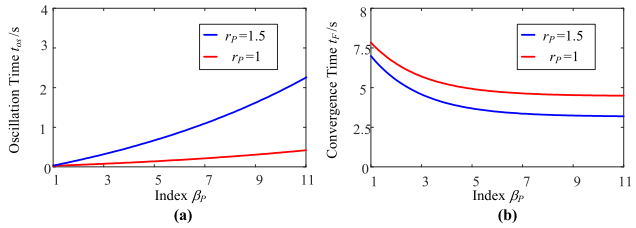


**FIGURE 9.** Oscillation time $t_{os}$ and convergence time $t_C$ versus index $\beta_P$ curves under the PDSC scheme in this paper. (a) $t_{os}$ $\beta_P$ curve. (b) $t_P$ $\beta_P$ curve.

than 10s, and having much larger transient overshoot. Thus, the TDSC scheme with saturation function possesses faster convergence speed than the general TDSC scheme. Moreover, it can also conclude that the PDSC scheme has better dynamic performance than the TDSC scheme when comparing the Fig. 6 with Fig. 5.

### 3) FDSC SCHEME WITH CHATTERING PHENOMENON

Under the same scenario we simulate the FDSC in [16] and [17] by setting the parameters as $k_2 = 3, k_3 = 1, \delta_P = 10$ for [16], and $k_4 = 1$, $k_5 = 0.05$ for [17]. Fig. 7(a1)-(c1) and Fig. 7(a2)-(c2) present the dynamics of FDSC in [16] and [17] with $\alpha_P = 0.5$, respectively. As seen, there are non-negligible chattering phenomena occurring, both for FDSC in [16] and [17]. Comparing with PDSC method in this paper, the FDSC algorithm in [16] is a timesaving convergence method, but there is always an inherent tradeoff between the chattering and convergence speed for a non-Lipchitz dynamic system. We further calculate the average active power chattering amplitudes $A_C$ under the different FDSC in [16] and [17] with the fractional index $\alpha_P$ increasing from 0 to 1, and the $A_C\alpha_P$ curves are depicted as Fig. 8(a). Moreover, Fig. 8(b) shows the relationship between the average active power finite convergence time $t_F$ and the fractional index $\alpha_P$. It is obvious that though smaller fractional index $\alpha_P$ means smaller finite convergence time $t_F$, the larger chattering will definitely occur.

As for the PDSC in this paper, we further evaluate the dynamics between oscillation time $t_{os}$, convergence time $t_C$ and index $\beta_P$ separately, which can be shown as Fig. 9. It is obvious that with the increasing of $\beta_P$, the convergence time is gradually reduced, but more oscillation will have. When comparing with Fig. 8, we are certain that the control method in this paper is a little more time-consuming than the FDSC in [16] and [17]. However, no chattering phenomenon is the main advantage of PDSC. Moreover, we can also have a relative higher scaling factor $r_P$, so that the convergence time

can be reduced, but the more oscillation goes. There is a tradeoff between less convergence time and less oscillation time.

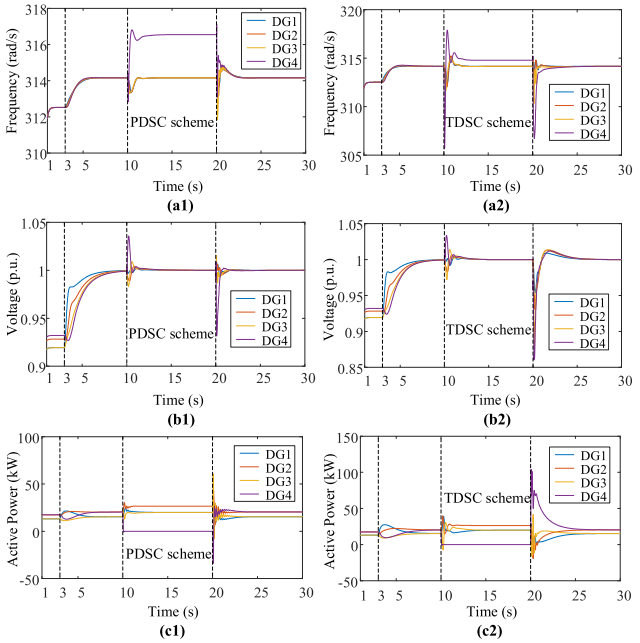


**FIGURE 10.** State outputs of plug in and play under PDSC scheme and TDSC scheme. (a1) and (a2) frequency response. (b1) and (b2) voltage response. (c1) and (c2) active power response.

### B. PLUG AND PLAY

The plug and play capability of the whole system is analyzed in Fig. 10, still using the comparison between PDSC and TDSC scheme. In all cases the switch of DG1 and DG4 are disconnected at t = 10s and reconnected at t = 20s. As seen in Fig. 9, the graph is still connected with DG1 receiving information from the leader node when DG4 is disconnected. Therefore, the algorithm can still work for the DG1, DG2 and DG3. Fig. 10 also shows that the system may endures dramatic transient overshoot when DG4 is reconnected. This is because no pre-synchronization is implemented. However, the transient frequency is kept in ±5% deviation and system can still keep stable even in this situation under PDSC and TDSC scheme. Still the dynamic performance of PDSC scheme is much better than the TDSC scheme.

### C. PERFORMANCE WITH TIME-DELAYS

In this section, the dynamic performance of the PDSC scheme is investigated under different communication time delays. The Fig. 11 shows that the more oscillation will happen when the communication time delays increasing. Considering the fact that the stability criteria is based on the Lyapunov theory, larger time delay will definitely diminish the stability region of the whole system. As we have stated in Section IV, in order to enlarge the tolerance of communication time-delay, we should choose a relatively smaller proportion constants, such as, $C_\omega = 2$, $C_V = 2$ and $C_P = 2$. In this

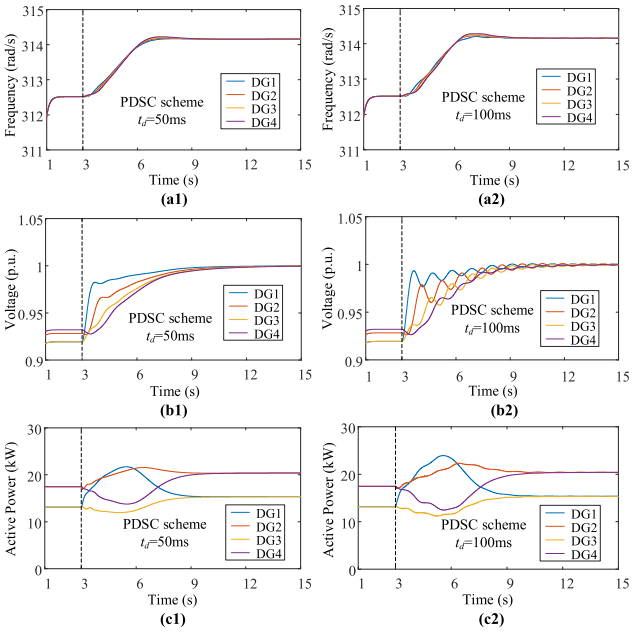


**FIGURE 11.** State outputs of PDSC scheme with $C_\omega = 2$, $C_V = 2$ and $C_P = 2$ under different communication time-delays. (a1) and (a2) frequency response. (b1) and (b2) voltage response. (c1) and (c2) active power response.

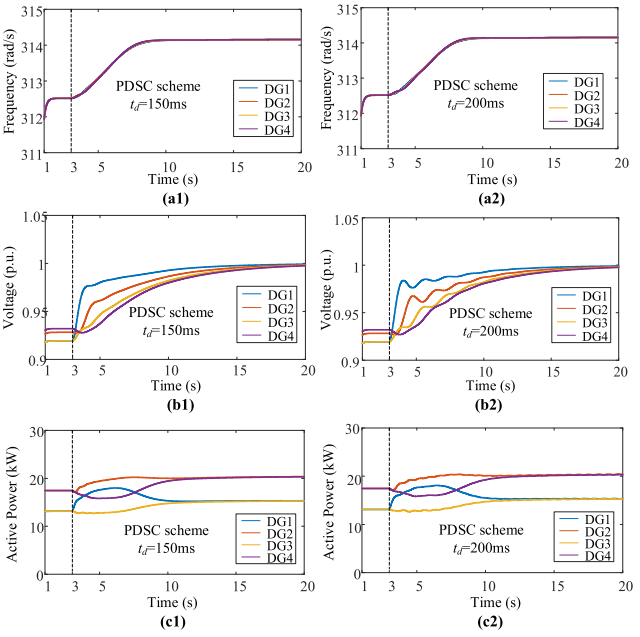


**FIGURE 12.** State outputs of PDSC scheme with $C_\omega = 1$, $C_V = 1$ and $C_P = 1$ under different communication time-delays. (a1) and (a2) frequency response. (b1) and (b2) voltage response. (c1) and (c2) active power response.

simulation, we can find that the system can remains stable under the cases of time-delay $t_d = 50$ms and 100ms, and the convergence speeds in both cases are reduced due to the smaller proportional gains.

We further reduce the proportional gains as $C_\omega = 1$, $C_V = 1$ and $C_P = 1$ and increase the time-delay to 150ms

and 200ms. The dynamic results can be seen in Fig. 12. It is obvious that the convergence speed is slower comparing with the cases in Fig. 12, but the tolerance for maximum time-delay is improved. Thus, we can always promote the resistance capability to the communication time-delay by scarifying the convergence speed and time.

Note that the time-delay of a common communication network will be approximately at milliseconds or tens of milliseconds, it is reasonable to conclude that the PDSC can realize the control requirements under the circumstance of time delay.

## VI. CONCLUSION

This paper proposes a novel nonlinear distributed secondary control strategy to achieve frequency restoration and accurate active power sharing in an islanded AC microgrid, while satisfying requirements of the bounded control input, the faster convergence speed and eliminating the chattering phenomenon. The stability issue of proposed DSC method is rigorously proved by using the Lyapunov method. The effectiveness of the control strategy is validated in the simulations with a test microgrid system. The future work will focus on the real-time simulation by using Dspace and further implement the PDSC method in a discrete way.

## APPENDIX

*Lemma 1:* If the Lyapunov function $V(y,t)$ are as (13), then $\dot{V}(y_i,t)$ can be presented as follow,

$$\dot{V}(y,t)=\sum_{i=1}^{n}\dot{V}(y_i,t)=-C_\omega r_\omega[1-(1-r_\omega sat_{1/r_\omega}|y|)^{\beta_\omega}]^T \times(\boldsymbol{L}^\omega+\boldsymbol{D}^\omega)[1-(1-r_\omega sat_{1/r_\omega}|y|)^{\beta_\omega}] \quad (23)$$

*Proof:* We first denote $V(y,t)$ as follow,

$$\begin{cases} V(y,t)=\sum_{i=1}^{n}V(y_i,t) \\ V(y_i,t)=r_\omega|y_i|-\dfrac{1}{\beta_\omega+1}(1-(1-r_\omega \mathrm{sat}_{1/r_\omega}|y_i|)^{\beta_\omega+1}) \end{cases} \quad (24)$$

It is easy to find that $V(y_i,t)$ is continuous at $y_i=0$, where $\lim_{y_i\to 0^+}V(y_i,t)=\lim_{y_i\to 0^-}V(y_i,t)=0$. Then, the differential function of $V(y_i,t)$ respect to $t$ can be presented as,

$$\dot{V}(y_i,t)=\begin{cases} r_\omega\ \mathrm{sign}(y_i)\dot{y}_i\left(1-(1-r_\omega|y_i|)^{\beta_\omega}\right) & |y_i|\le 1/r_\omega \\ r_\omega\ \mathrm{sign}(y_i)\dot{y}_i & |y_i|>1/r_\omega \end{cases} \quad (25)$$

It is obvious that $\lim_{y_i\to 0^+}\dot{V}(y_i,t)=\lim_{y_i\to 0^-}\dot{V}(y_i,t)=0$. So that we can conclude that, the function $V(y_i,t)$ is a regular, continuous and Lipschitz function at 0. Moreover, the saturation function sat() is defined as follow,

$$sat_{1/r}(u)=\begin{cases} u & |u|\le\dfrac{1}{r} \\ \mathrm{sign}(u)\dfrac{1}{r} & |u|>\dfrac{1}{r} \end{cases} \quad (26)$$

We can also write $\dot{V}(y_i,t)$ as,

$$\dot{V}(y_i,t)=r_\omega\ \mathrm{sign}(y_i)\dot{y}_i\left(1-(1-r_\omega \mathrm{sat}_{1/r_\omega}|y_i|)^{\beta_\omega}\right) \quad (27)$$

Note here $\dot{y}_i$ can be further presented as,

$$\dot{y}_i=-C_\omega \boldsymbol{L}_{iN}^\omega\ sign(y)(1-(1-r_\omega \mathrm{sat}_{1/r_\omega}(|y|))^{\beta_\omega}) \quad (28)$$

where $\boldsymbol{L}_{iN}^\omega$ is the column vector $i$ of the Laplace matrix $\boldsymbol{L}^\omega+\boldsymbol{D}^\omega$, so that we combine (24)-(28) and obtain (29) as follow,

$$\dot{V}(y,t)=\sum_{i=1}^{n}\dot{V}(y_i,t)=-C_\omega r_\omega[1-(1-r_\omega sat_{1/r_\omega}|y|)^{\beta_\omega}]^T \times(\boldsymbol{L}^\omega+\boldsymbol{D}^\omega)[1-(1-r_\omega \mathrm{sat}_{1/r_\omega}|y|)^{\beta_\omega}] \quad (29)$$

where (29) equals to (23) and the proof is complete.

*Lemma 2 ([22], [24]):* Graph Laplacian $\boldsymbol{L}(\boldsymbol{A})$ of $\boldsymbol{G}(\boldsymbol{A})$ has the following properties:

A undirected graph $\boldsymbol{G}(\boldsymbol{A})$ is called connected if and only if $\mathrm{rank}(\boldsymbol{L}(\boldsymbol{A}))=n-1$.

A weighted digraph $\boldsymbol{G}(\boldsymbol{A})$ is called strongly connected if there is a directed path between any two nodes and exists a positive column vector $\boldsymbol{w}\in R^N$ such that $\boldsymbol{w}^T\boldsymbol{L}(\boldsymbol{A})=0$. Moreover, if at least one node can access to the leader node, $\boldsymbol{L}(\boldsymbol{A})+\boldsymbol{D}(\boldsymbol{A})$ is a positive definite matrix where $\boldsymbol{D}=diag\{a_i\}$

*Lemma 3:* A real-valued function f: $\boldsymbol{R}\to\boldsymbol{R}$ is called Lipschitz continuous if there exists a positive real constant $K$ such that, for all real $x_1$ and $x_2$, $|f(x_1)-f(x_2)|\le K|x_1x_2|$, In general, if the derivative of f as a function is bounded, then f will be Lipschitz continuous. In addition, as an additional note if a function f defined on $\boldsymbol{S}\subseteq\boldsymbol{R}$ is Lipschitz continuous then f is uniformly continuous on $\boldsymbol{S}$

*Lemma 4:* Consider the initial value problem

$$y'(t)=f(t,y(t)),\quad y(t_0)=y_0$$

Suppose $f$ is uniformly Lipschitz continuous in y (meaning the Lipschitz constant can be taken independent of $t$) and continuous in $t$. Then, for some value $\varepsilon>0$, there exists a unique solution $y(t)$ to the initial value problem on the interval $[t_0-\varepsilon,t+\varepsilon]$.

## REFERENCES

[1] N. Pogaku, M. Prodanovic, and T. C. Green, "Modeling, analysis and testing of autonomous operation of an inverter-based microgrid," *IEEE Trans. Power Electron.*, vol. 22, no. 2, pp. 613–625, Mar. 2007.
[2] J. M. Guerrero, J. C. Vasquez, J. Matas, L. G. de Vicuna, and M. Castilla, "Hierarchical control of droop-controlled AC and DC microgrids—A general approach toward standardization," *IEEE Trans. Ind. Electron.*, vol. 58, no. 1, pp. 158–172, Jan. 2011.
[3] J. M. Guerrero, M. Chandorkar, T.-L. Lee, and P. C. Loh, "Advanced control architectures for intelligent microgrids—Part I: Decentralized and hierarchical control," *IEEE Trans. Ind. Electron.*, vol. 60, no. 4, pp. 1254–1262, Apr. 2013.
[4] A. Bidram and A. Davoudi, "Hierarchical structure of microgrids control system," *IEEE Trans. Smart Grid*, vol. 3, no. 4, pp. 1963–1976, Dec. 2012.
[5] C. Ahumada, R. Cárdenas, D. Sáez, and J. M. Guerrero, "Secondary control strategies for frequency restoration in islanded microgrids with consideration of communication delays," *IEEE Trans. Smart Grid*, vol. 7, no. 3, pp. 1430–1441, May 2016.
[6] K. T. Tan, X. Y. Peng, P. L. So, Y. C. Chu, and M. Z. Q. Chen, "Centralized control for parallel operation of distributed generation inverters in microgrids," *IEEE Trans. Smart Grid*, vol. 3, no. 4, pp. 1977–1987, Dec. 2012.

[7] P. N. Vovos, A. E. Kiprakis, A. R. Wallace, and G. P. Harrison, "Centralized and Distributed Voltage Control: Impact on Distributed Generation Penetration," *IEEE Trans. Power Syst.*, vol. 22, no. 1, pp. 476–483, Feb. 2007.

[8] Q. Shafiee, J. M. Guerrero, and J. C. Vasquez, "Distributed secondary control for islanded microgrids–A novel approach," *IEEE Trans. Power Electron.*, vol. 29, no. 2, pp. 1018–1031, Feb. 2014.

[9] M. Savaghebi, A. Jalilian, J. C. Vásquez, and J. M. Guerrero, "Secondary control for voltage quality enhancement in microgrids," *IEEE Trans. Smart Grid*, vol. 3, no. 4, pp. 1893–1902, Dec. 2012.

[10] N. M. Dehkordi, N. Sadati, and M. Hamzeh, "Fully distributed cooperative secondary frequency and voltage control of islanded microgrids," *IEEE Trans. Energy Convers.*, vol. 32, no. 2, pp. 675–685, Jun. 2017.

[11] M. Chen, X. Xiao, and J. M. Guerrero, "Secondary restoration control of islanded microgrids with a decentralized event-triggered strategy," *IEEE Trans. Ind. Informat.*, vol. 14, no. 9, pp. 3870–3880, Sep. 2018. doi: 10.1109/TII.2017.2784561.

[12] A. Bidram, A. Davoudi, F. L. Lewis, and J. M. Guerrero, "Distributed cooperative secondary control of microgrids using feedback linearization," *IEEE Trans. Power Syst.*, vol. 28, no. 3, pp. 3462–3470, Aug. 2013.

[13] N. M. Dehkordi, N. Sadati, and M. Hamzeh, "Distributed robust finite-time secondary voltage and frequency control of islanded microgrids," *IEEE Trans. Power Syst.*, vol. 32, no. 5, pp. 3648–3659, Sep. 2017.

[14] A. Bidram, A. Davoudi, F. L. Lewis, and Z. Qu, "Secondary control of microgrids based on distributed cooperative control of multi-agent systems," *IET Generat., Transmiss., Distrib.*, vol. 7, no. 8, pp. 822–831, Aug. 2013.

[15] X. Wang, H. Zhang, and C. Li, "Distributed finite-time cooperative control of droop-controlled microgrids under switching topology," *IET Renew. Power Gener.*, vol. 11, no. 5, pp. 707–714, Apr. 2017.

[16] X. Lu, X. Yu, J. Lai, Y. Wang, and J. M. Guerrero, "A novel distributed secondary coordination control approach for islanded microgrids," *IEEE Trans. Smart Grid*, vol. 9, no. 4, pp. 2726–2740, Jul. 2018.

[17] Z. Deng, Y. Xu, H. Sun, and X. Shen, "Distributed, bounded and finite-time convergence secondary frequency control in an autonomous microgrid," *IEEE Trans. Smart Grid*, to be published.

[18] X. Lu, Y. Wang, X. Yu, and J. Lai, "Finite-time control for robust tracking consensus in MASs with an uncertain leader," *IEEE Trans. Cybern.*, vol. 47, no. 5, pp. 1210–1223, May 2017.

[19] X. Lu, R. Lu, S. Chen, and J. Lü, "Finite-time distributed tracking control for multi-agent systems with a virtual leader," *IEEE Trans. Circuits Syst. I, Reg. Papers*, vol. 60, no. 2, pp. 352–362, Feb. 2013.

[20] G. Chen, F. L. Lewis, and L. Xie, "Finite-time distributed consensus via binary control protocols," *Automatica*, vol. 47, no. 9, pp. 1962–1968, Sep. 2011.

[21] Y. Xu, "Robust finite-time control for autonomous operation of an inverter-based microgrid," *IEEE Trans. Ind. Informat.*, vol. 13, no. 5, pp. 2717–2725, Oct. 2017.

[22] R. Olfati-Saber and R. M. Murray, "Consensus problems in networks of agents with switching topology and time-delays," *IEEE Trans. Autom. Control*, vol. 49, no. 9, pp. 1520–1533, Sep. 2004.

[23] J. Qi, J. Wang, H. Liu, and A. D. Dimitrovski, "Nonlinear model reduction in power systems by balancing of empirical controllability and observability covariances," *IEEE Trans. Power Syst.*, vol. 32, no. 1, pp. 114–126, Jan. 2017.

[24] F. Xiao, J. Chen, and L. Wang, "Finite-time formation control for multi-agent systems," *Automatica*, vol. 45, no. 11, pp. 2605–2611, 2009.

[25] S. P. Bhat and D. S. Bernstein, "Lyapunov analysis of finite-time differential equations," in *Proc. Amer. Control Conf. (ACC)*, Seattle, WA, USA, vol. 3, Jun. 1995, pp. 1831–1832.

[26] S. P. Bhat and D. S. Bernstein, "Continuous finite-time stabilization of the translational and rotational double integrators," *IEEE Trans. Autom. Control*, vol. 43, no. 5, pp. 678–682, May 1998.


**XIAOXIAO MENG** received the B.S. degree in electrical engineering from Chongqing University, Chongqing, China, in 2014, where he is currently pursuing the Ph.D. degree in electrical engineering. From 2017 to 2018, he was a Visiting Research Student with Aalborg University, Denmark. His research interests include power system stability analysis, distributed generation, and microgrids.

**NIANCHENG ZHOU** (M'18) received the B.S., M.S., and Ph.D. degrees in electrical engineering from Chongqing University, Chongqing, China, in 1991, 1994, and 1997, respectively, where he is currently a Professor with the School of Electrical Engineering. He was with Chongqing Kuayue Technology Co, Ltd., from 1997 to 2003. From 2010 to 2011, he was a Research Fellow with Nanyang Technological University, Singapore. His research interests include analysis, operation of power systems, microgrid, and power quality.

**QIANGGANG WANG** (S'13–M'15) received the B.S. and Ph.D. degrees in electrical engineering from Chongqing University, Chongqing, China, in 2009 and 2015, respectively, where he is currently an Associate Professor. From 2015 to 2016, he was a Research Fellow with Nanyang Technological University, Singapore. His research interests include power system operation, microgrids, and power quality.

**JOSEP M. GUERRERO** (S'01–M'04–SM'08–FM'15) received the B.S. degree in telecommunications engineering, the M.S. degree in electronics engineering, and the Ph.D. degree in power electronics from the Technical University of Catalonia, Barcelona, in 1997, 2000, and 2003, respectively. Since 2011, he has been a Full Professor with Aalborg University, Denmark. He has published more than 450 journal papers in the fields of microgrids and renewable energy systems, which are cited more than 30,000 times. His research interests include power electronics, distributed systems, hierarchical and cooperative control, and the Internet of Things for AC/DC microgrid; recently specially focused on maritime microgrids for electrical ships, vessels, ferries and seaports. During five consecutive years, from 2014 to 2018, he was awarded as Highly Cited Researcher. He is an Associate Editor for a number of IEEE TRANSACTIONS.